Supplementary information

Pressure regulated CO_2 electrolysis on two-dimensional Bi_2O_2Se

Ruofan Sun,[a]† Jiwu Zhao,[a]† Hang Liu,[a] Yanrong Xue,[a] Xu Lu[a]*

[a] Division of Physical Science and Engineering (PSE), King Abdullah University of Science and Technology (KAUST), Thuwal, 23955-6900, Kingdom of Saudi Arabia.

† These authors contributed equally.

* Corresponding author. Email: Xu Lu (xu.lu@kaust.edu.sa).

Experimental

Catalyst synthesis and electrode preparation

A homemade CVD furnace was utilized to grow the 2D Bi_2O_2Se on a glassy carbon substrate under low pressure conditions. Initially, a 10 nm layer of Bi_2O_3 was deposited onto the glassy carbon substrate at a rate of 0.01 nm/s using an E-beam evaporator (Denton Vacuum, LLC), with Bi_2O_3 powder (99.99% purity, Alfa) as the source material. Subsequently, the glassy carbon substrate with the deposited Bi_2O_3 and 1 g of Se powder (99.99% purity, Alfa) were positioned in the central and upstream heating zones of the furnace, approximately 10 cm from the center. Prior to heating the furnace, the quartz tube was purged with 1000 sccm of Ar for 5 minutes. Subsequently, the furnace temperature was ramped up to 500°C at a rate of 5°C/min and held constant for 20 minutes with a continuous flow of Ar at 200 sccm to conduct the selenization process. The pressure was maintained at 200 Torr throughout the entire CVD process. The Bi_2O_2Se bulk were synthesized with a similar method. In brief, 10mg Bi_2O_3 and 1 g of Se powder were positioned in furnace to conduct the selenization process. Two milligrams of prepared Bi_2O_2Se bulk were first dispersed in 1 mL of ethanol (EtOH) with the addition of 20 µL of a 5 wt% Nafion solution. This suspension was then dropped cast onto the glassy carbon with the catalyst loading of 0.5 mg cm^{-2}. All the catalyst electrodes were tested with an active area of 1cm^2.

Electrochemical measurement

All electrochemical measurements were performed at room temperature using an electrochemical workstation (BioLogic SP-150 Potentiostat). A Pt foil served as the counter electrode and an Ag/AgCl electrode (saturated KCl) was used as the reference electrode. All potentials recorded against the Ag/AgCl reference electrode (without iR correction) were converted to the reversible hydrogen electrode (RHE) scale using the formula: $E_{RHE} = E_{Ag/AgCl} + 0.21\ V + 0.0591 * pH$, where pH represents the pH value of the solution.

For high-pressure measurements, we utilized a customized two-compartment high-pressure H-cell constructed from Teflon-lined titanium as previous work[1]. The two compartments were separated by a proton exchange membrane (Nafion 117, Fuel Cell Store), with each containing 100 mL of 0.5M $KHCO_3$ aqueous solution and connected to an independent pressure regulator. Inside the cathode compartment, the working electrode (1 × 0.5 cm) and reference electrode (Ag/AgCl with saturated KCl, Gaoss Union) were placed, while the counter electrode (Pt foil, 1 × 1 cm) was located in the anode compartment. A small hole was drilled on the top of the reference electrode to balance its internal and external pressure. Before conducting tests, the electrolytes in each compartment were purged for 5 minutes using CO_2 and then allowed to equilibrate for 30 minutes under the desired pressure (ranging from 1 to 40 bar). Gas products in the headspace of the cathode compartment were sampled using 10 mL air-tight syringes from an outlet relief valve and then injected into a gas chromatograph (GC) system.

The determination of electrolyte pH at high pressure

Step 1: Calculate dissolved CO_2 concentration using Henry's Law

$[CO_2] = K_H \cdot P_{(CO2)}$

Step 2: Determine carbonic acid concentration

$$\frac{a}{b} + \frac{c}{d} = \frac{[CO_2]}{1 + \frac{[H^+]}{K_{a1}}}$$

$[H_2CO_3] = [CO_2]$, where $K_{a1} = 4.3\times10^{-7}$.

Step 3: Calculate bicarbonate concentration

$[H^{CO}{}_3^-] = [H_2CO_3] * \frac{K_{a1}}{[H^+]} * C_{KHCO_3}$, where $C_{KHCO_3} = 0.5M$ is the initial bicarbonate concentration.

Step 4: Calculate carbonate concentration

$[{}^{CO^2}{}_3^-] = [H^{CO}{}_3^-] * \frac{K_{a2}}{[H^+]}$, where $K_{a2} = 4.8\times10^{-11}$.

Step 5: Charge balance equation

$[H^+]+[K^+]=[OH^-]+[HCO_3^-]+2[CO_3^{2-}]$

Step 6: Iterative solution for $[H^+]$

Use the equation above to solve for $[H^+]$.

Step 7: Calculate pH= $-\mathrm{Log}_{10}([H^+])$

Product analysis

Gas products were analyzed using a GC (Trace 1310, Thermo Scientific) equipped with Molecular Sieve 5A and Porapak columns. Ar (Al Khafrah Industrial Gases, 99.999%) served as the carrier gas. CO, CH_4, C_2H_4, and C_2H_6 were quantified using a flame ionization detector (FID) with a methanizer, while H_2 was quantified using a thermal conductivity detector (TCD). The gas in the compartment's headspace were collected using 10 mL air-tight syringes via an outlet relief valve and analyzed with a gas chromatograph (GC) system. The volumes of the gas products were determined by analyzing the corresponding peak areas with reference to calibration curves. Liquid products were detected by a 1H NMR spectrometer (Bruker, 600 MHz) employing the water suppression method. For each liquid sample, 480 µL of the electrolytes were mixed with 120 µL of internal standards, consisting of 200 ppm of dimethyl sulfoxide (DMSO) in deuterium oxide (D_2O) and distilled water.

The Faradaic efficiency (FE) of a specific product (p) was calculated using the equation:

$$FE(p)=\frac{z*n*F}{Q}*100(\%)$$

where z represents the number of the electrons transferred to one p molecule, n denotes the total moles of the product, F is the Faradaic constant (F = 96,485 C mol^{-1}), and Q indicates the total number of electrons transferred.

Electrochemically active surface areas (ECSA) calculation

The electrochemically active surface area (ECSA) is calculated using the formula ECSA = Rf*S. Here, S denotes the real surface area of the smooth metal electrode, which generally equals the geometric area of the carbon paper electrode (S = 1.0 cm^2 in this study). The roughness factor (Rf) is derived from the ratio of the double-layer capacitance (Cdl) of the working electrode to that of a smooth metal electrode.

Assuming an average double-layer capacitance of 21 µF cm^{-2} for a carbon-supported metal surface, Rf is determined as Rf=Cdl/(21 µF cm^{-2}).

To determine Cdl, the capacitive current associated with double-layer charging is measured from the scan-rate dependence of cyclic voltammetric stripping. The potential window for cyclic voltammetric stripping is set between 0.3 and 0.4 V versus RHE in a 0.5 M $KHCO_3$ solution, with scan rates of 10, 20, 30, 50, 80, and 100 mV s^{-1}.

The estimation of Cdl involves plotting the change in current density (Δj = ja - jc) at 0.35 V (where ja and jc are the anodic and cathodic current densities, respectively) against the scan rate. The slope of this plot provides a value that is twice that of Cdl.

Materials characterization and in-situ Raman measurement

High-resolution transmission electron microscopy (HR-TEM) and electron energy loss spectroscopy (EELS) images were acquired using an aberration-corrected transmission electron microscope (TEM) equipped with a post-column EELS system. The microscope, with a Cs probe, was from ThermoFisher Scientific, while the EELS equipment, model GIF-Quantum 966, was from Gatan, Inc. The analysis was conducted at an operating voltage of 300 kV.

The thickness and surface topology of Bi_2O_2Se were identified through AFM (Bruker Dimension Icon).

X-ray photoelectron spectroscopy (XPS) characterization was performed using a Kratos Analytical AMICUS/ESCA 3400 instrument equipped with an Mg-anode Kα excitation X-ray source (*hv* = 1253.6 eV) at 10 kV and 10 mA. Binding energies of the elements were referenced to the C 1s peak at 284.8 eV.

In-situ Raman spectra were collected using a WITec apyron system equipped with a 633 nm laser beam and a water-immersion objective lens (Zeiss W Plan-Apochromat 63X/1) in a customized cell according to previous reported work[1]. To prevent laser-induced surface modification of the catalyst, a power of 30 mW was applied. In the customized in-situ Raman cell, a Pt wire served as the working electrode (CE), an Ag/AgCl electrode (saturated KCl solution) as the reference electrode (RE), and the cathode and anode compartments were separated by a Fumasep FKB-PK-130 membrane (Fuel Cell Store). For test at 1.01 bar, the electrolyte (50 mL 0.5 M KCl) was circulated to the cathode compartment at a flow rate of 2 mL/min. For test at high pressure at 20 bar, we designed a high-pressure Raman cell according to previous reported work[2], as shown in Fig. S21. The cell was housed in a stainless-steel shell capable of withstanding pressures up to 20 atm. It featured a 3 cm × 3 cm window designed for optical measurements. For standard high-pressure in situ Raman spectroscopy experiments, a 1 cm × 1 cm electrode was affixed to the working electrode substrate using double-sided copper tape. $KHCO_3$ solution was then introduced into the cell. Once the stainless-steel shell was sealed, high pressure was supplied from a CO_2 cylinder, followed by the application of reduction potential.

ICP-MS (Agilent, 8800) was used to determine the contents of Bi_2O_2Se for as-prepared catalysts. Prior to ICP-MS measurements, the electrode was digested by an Ultrawave (Milestone, SRC Technology) in HNO_3 for 6 h. The final Bi_2O_2Se amount was estimated as: $m=C_{(Bi)}/2*Mw_{(Bi2O2Se)}$, where the $C_{(Bi)}$ is the concentration of Bi and $Mw_{(Bi2O2Se)}$ is molecule weight of Bi_2O_2Se.

DFT calculation

Density functional theory (DFT) calculations were performed using the Vienna Ab initio Simulation Program (VASP)[3-5]. Core-valence interactions were calculated using the projector augmented wave (PAW) method[6, 7]. The generalized gradient approximation within the Perdew–Burke–Ernzerhof functional (GGA-PBE) was employed to account for the exchange-correlation effects[8]. Additionally, the DFT-D3 method was utilized to incorporate dispersion corrections for van der Waals forces[9]. Convergence in geometry optimization was reached when the force on each atom fell below 0.02 eV Å−1. According to the experiment facts, Bi (012) facet is employed as the activate surface to convert CO_2 to HCOOH, with different CO_2 coverages of 1/8 (ambient pressure) and 3/8 (high pressure), respectively. A vacuum layer of 18 Å was introduced to eliminate the interaction between two adjacent slabs. The Brillouin zone sampling was performed using Gamma-centered Monkhorst-Pack (MP) grids[10], and the k-point was set as 3*3*1 for all the DFT calculations. The data processing was assisted by VASPKIT[11], QVASP[12] and VESTA[13] software. The Gibbs free energy difference (ΔG) between initial and final states was denoted as:

$$\Delta G = \Delta E + \Delta ZPE - T\Delta S$$

where E, ZPE, T and S represent the energy from DFT calculation, zero-point energy, temperature (298.15 K) and entropy, respectively[14, 15].

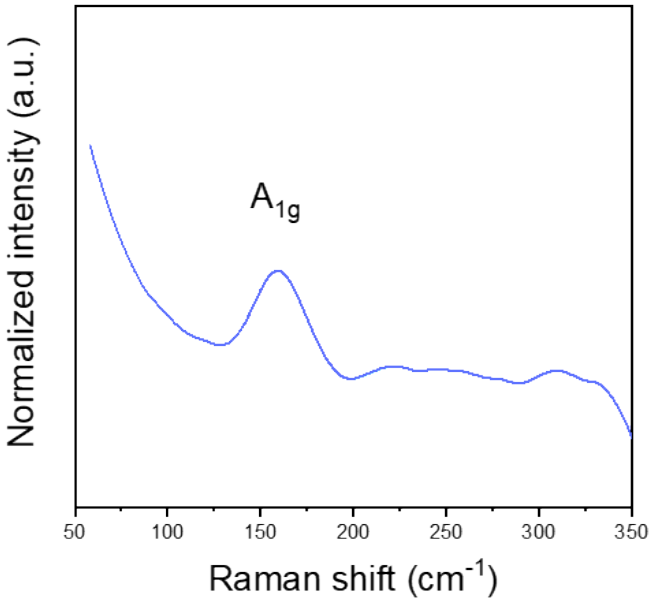

Fig. S1 Raman characterization on 2D Bi_2O_2Se.

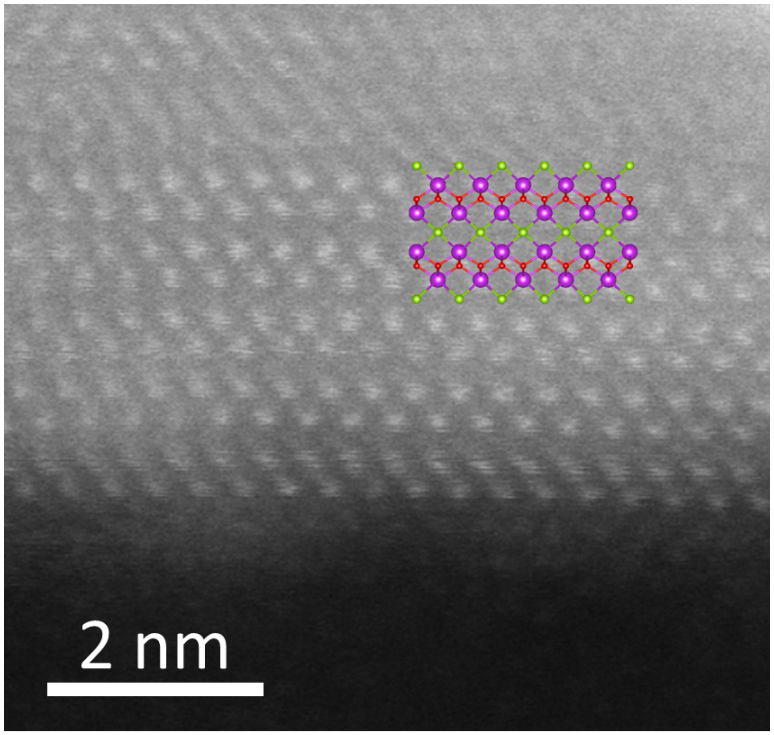

Fig. S2 Cross-sectional HAADF-STEM image of a Bi_2O_2Se.

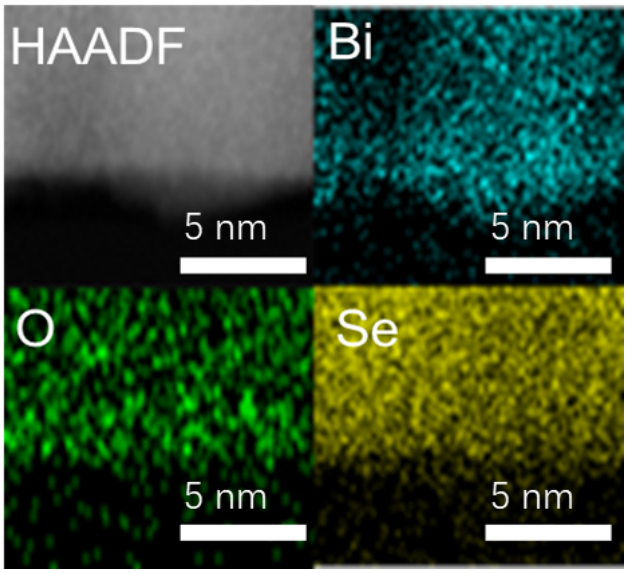

Fig. S3 The corresponding EELS elemental mapping of Bi, O, Se elements.

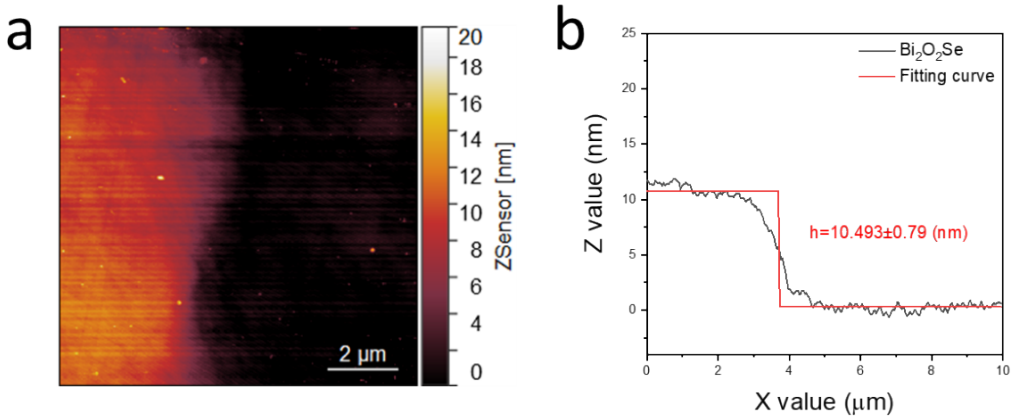

Fig. S4. (a) Typical atomic force microscopy (AFM) mapping and (b) thickness fitting.

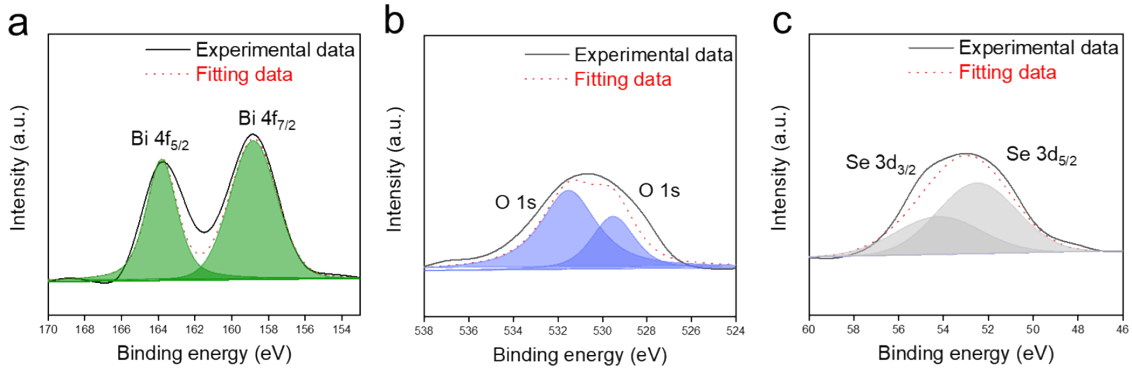

Fig. S5 XPS analysis of (a) Bi, (b) O and (c) Se elements.

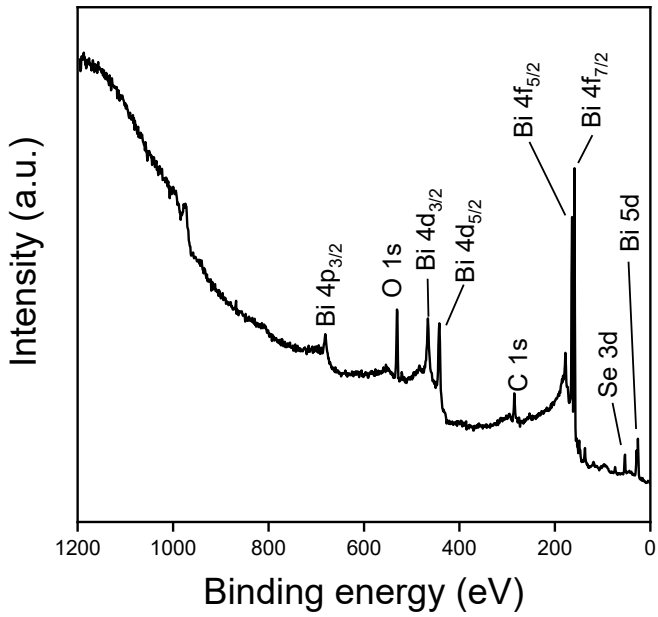

124

125 Fig. S6 X-ray photoelectron spectroscopy (XPS) analysis of wide spectrum.

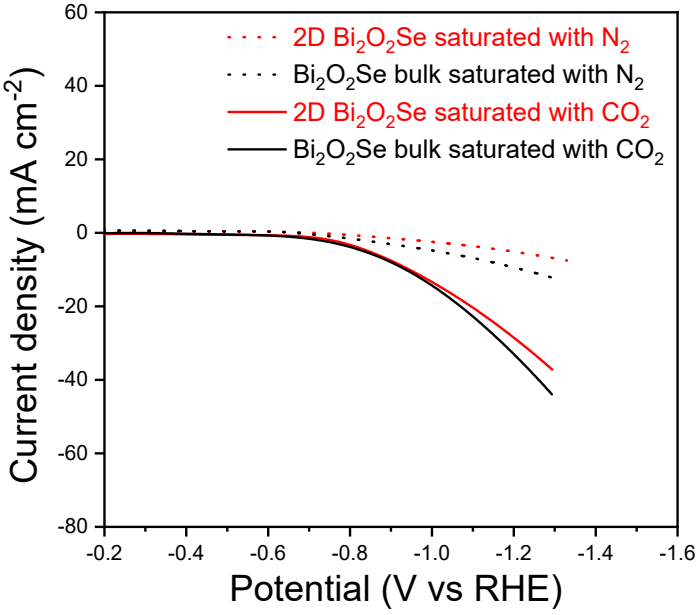

126

127 Fig. S7 Non-Mass-Normalized LSV of 2D Bi_2O_2Se and Bi_2O_2Se bulk saturated with CO_2 and N_2.

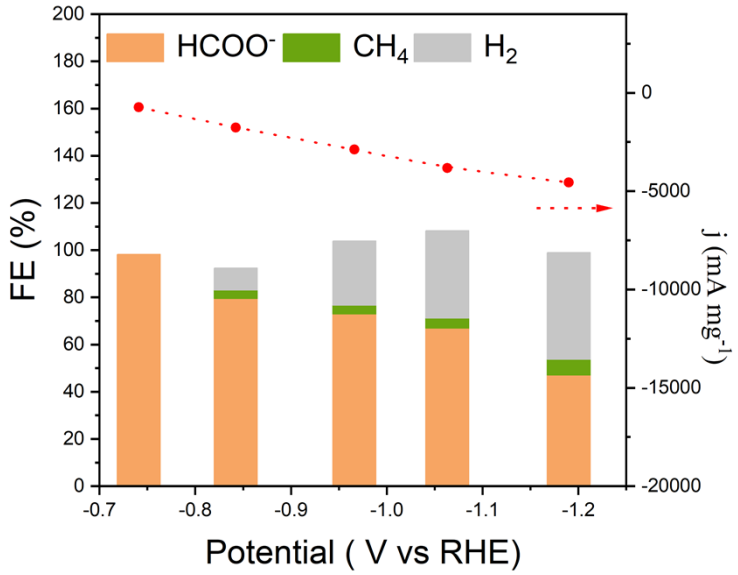

Fig. S8 FE and current density over 2D Bi_2O_2Se at atmosphere pressure.

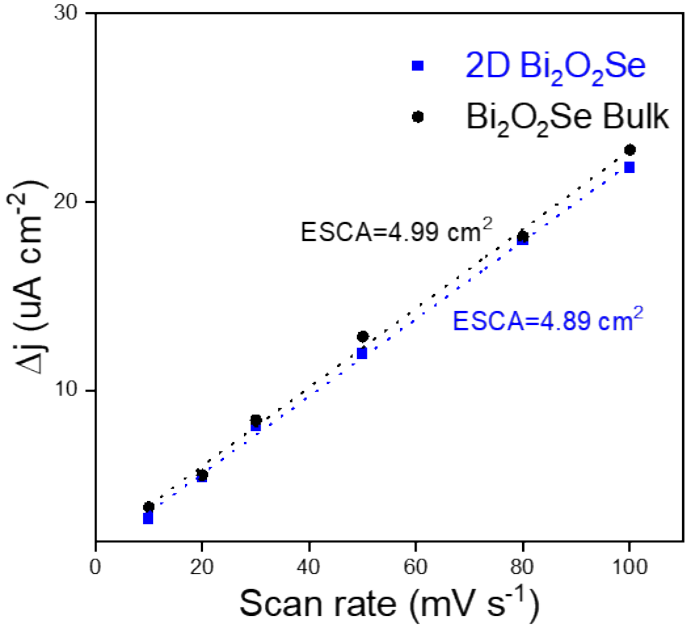

Fig. S9 Charging current density differences Δj plotted against scan rates on for the calculation of ECSA.

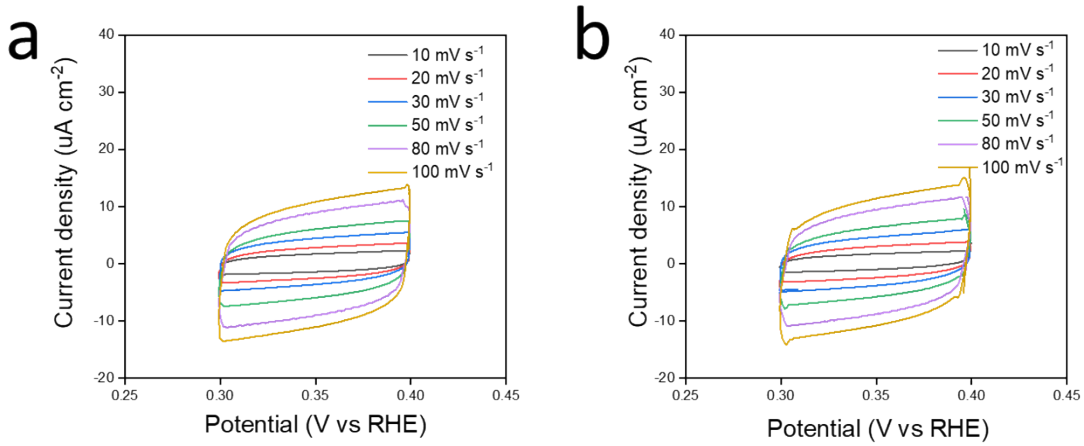

Fig. S10 Cyclic voltammograms of (a) 2D Bi_2O_2Se and (b) Bi_2O_2Se bulk within the potential range from -0.4 to -0.3 (V vs RHE) in 0.5 M $KHCO_3$ electrolyte.

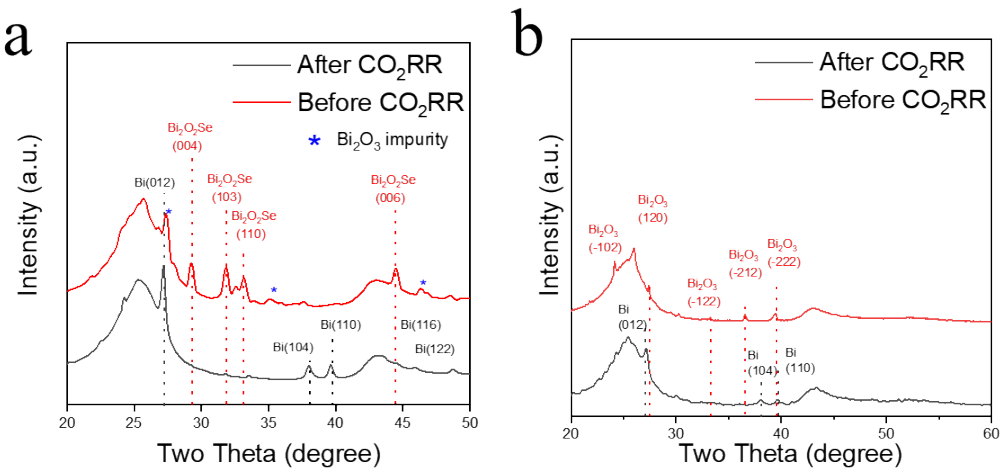

Fig. S11 XRD measurement before and after CO_2RR for 30 min over (a) Bi_2O_2Se bulk and (b) Bi_2O_3 bulk. For XRD measurement, we measured the bulk catalyst electrode due to the weak signal form 2D materials. The peak marked with * is originated from Bi_2O_3 reactant during the CVD synthesis.

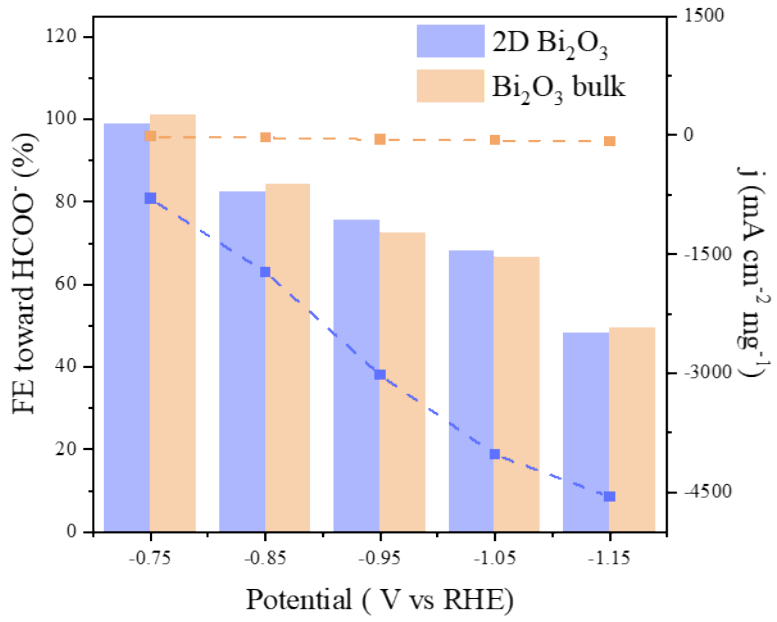

139

140 Fig. S12 CO_2RR to $HCOO^-$ performance of 2D Bi_2O_3 and Bi_2O_3 bulk at 1.01 bar.

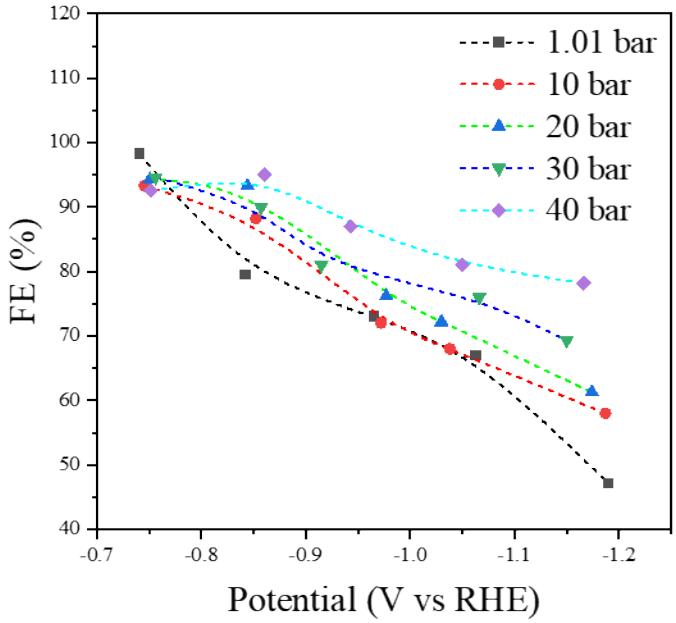

141

142 Fig. S13 Formate FE under CO_2 pressure regulation.

143

144

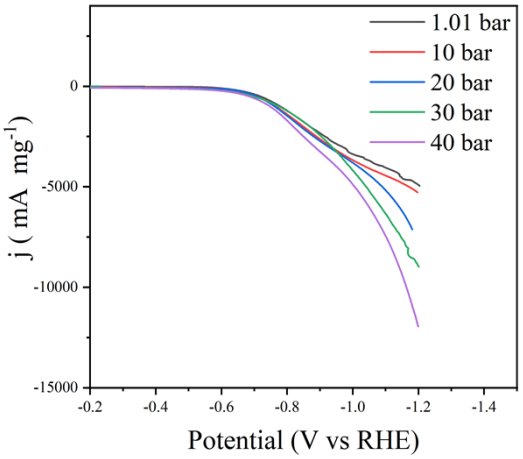

145

146 Fig. S14 LSV of 2D Bi_2O_2Se catalyst in CO_2 saturated electrolyte at different CO_2 pressure.

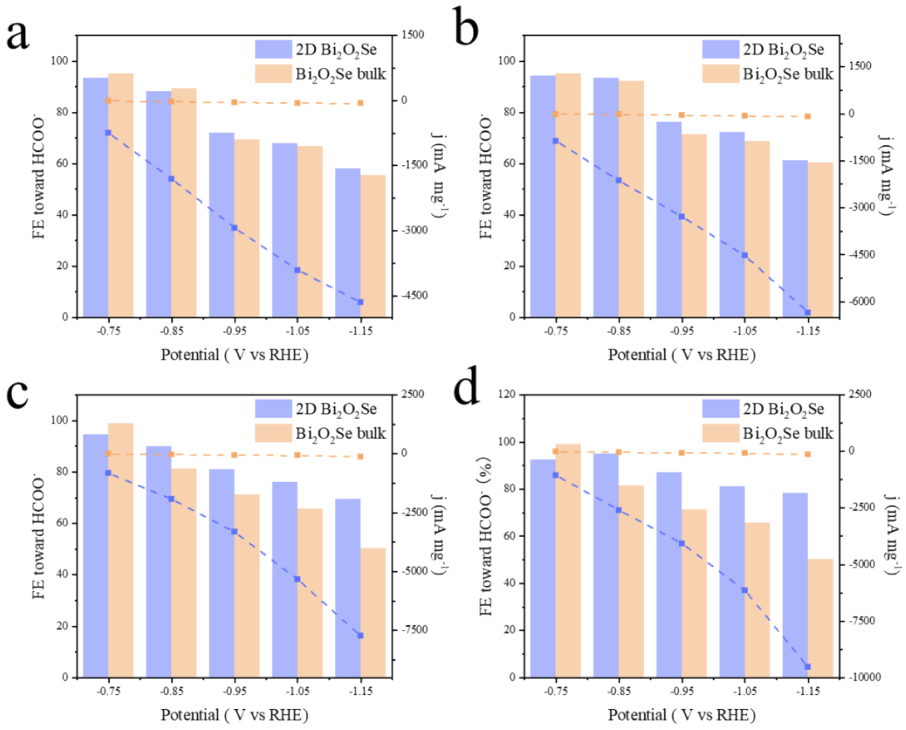

147

148 Fig. S15. FEs and current densities toward CO_2RR products at (a) 10 bar, (b) 20 bar, (c) 30 bar and (d) 40 bar CO_2 pressure.

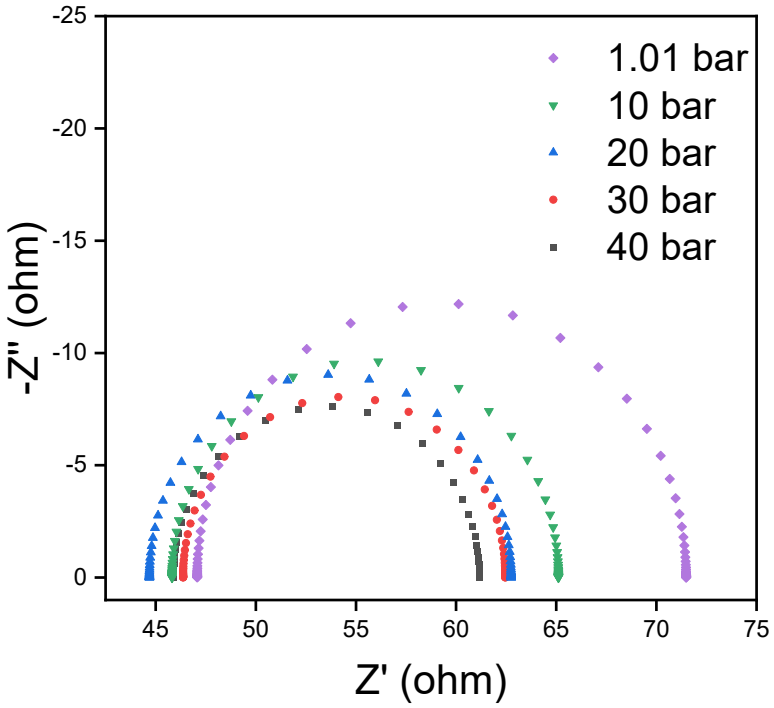

149

150 Fig. S16 Nyquist plots for CO_2RR over 2D Bi_2O_2Se catalyst with increased CO_2 pressure.

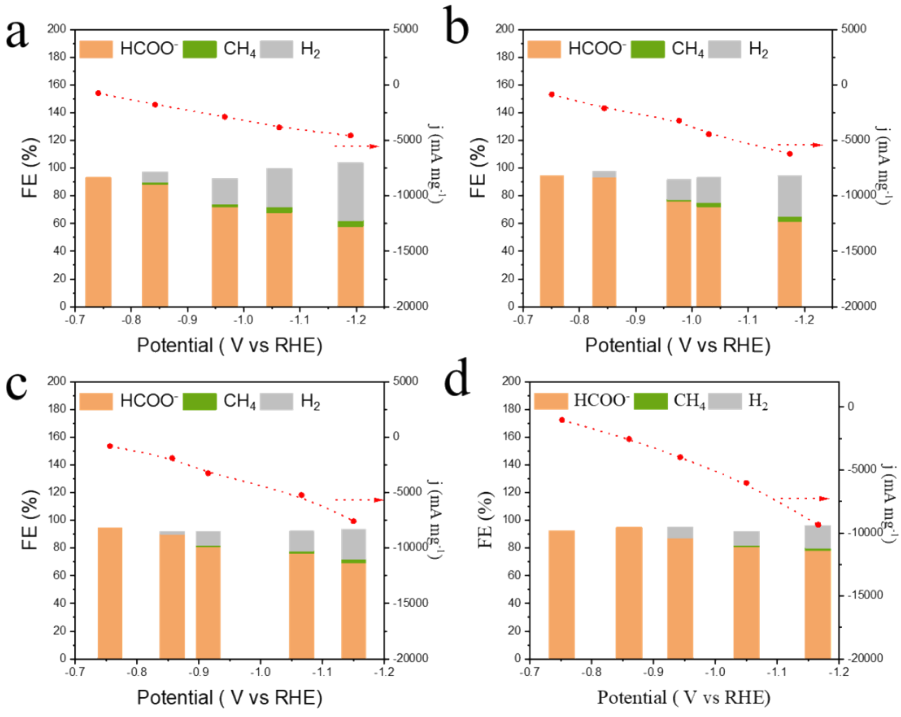

151

152 Fig. S17 FE and current density over 2D Bi_2O_2Se at (a) 10 bar, (b) 20 bar, (c) 30 bar and (d) 40 bar CO_2 pressure.

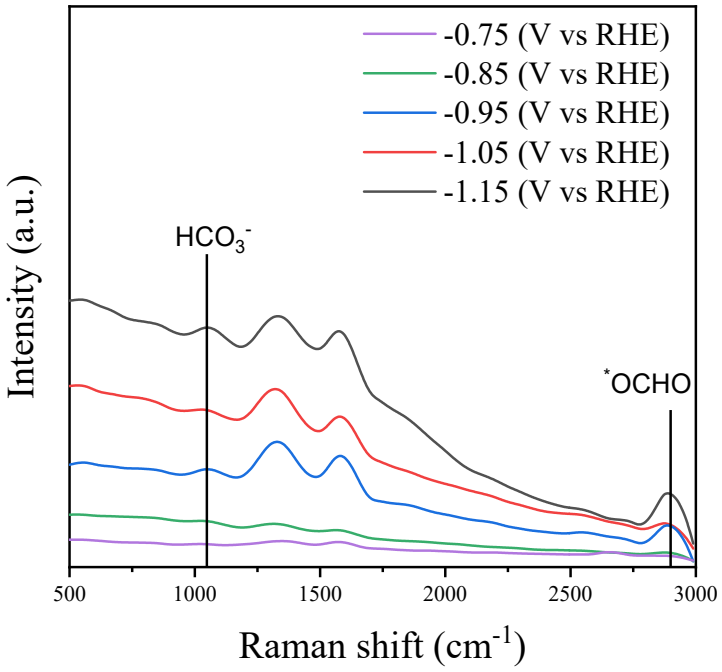

153

154 Fig. S18 *In-situ* Raman analysis on CO_2RR to $HCOO^-$ intermediates over 2D Bi_2O_2Se.

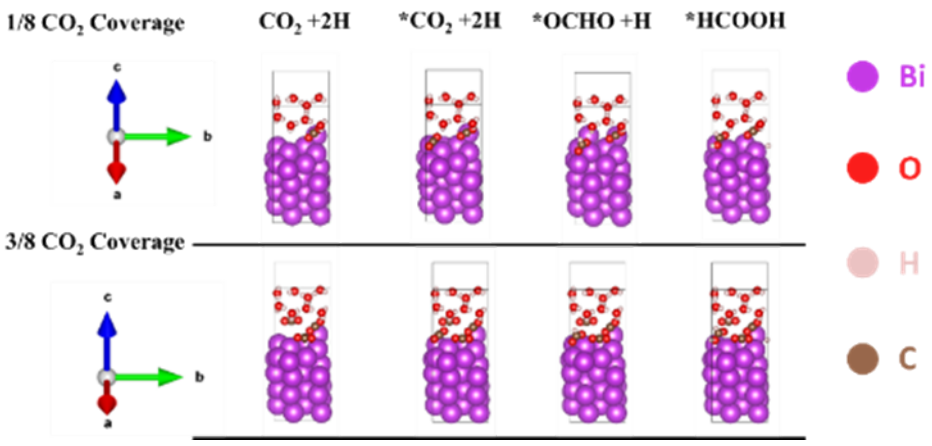

155

156 Fig. S19 Optimized of adsorbed CO2RR intermediates with the CO_2 coverages of 1/8 ML and 3/8 ML.

157

158

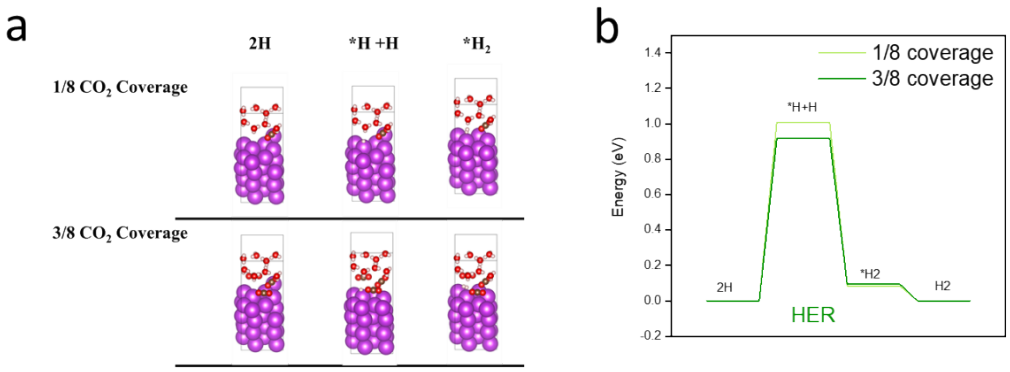

159

160 Fig. S20. (a) Optimized structure and (b) of adsorbed HER intermediates with the CO_2 coverages of 1/8 ML and 3/8 ML.

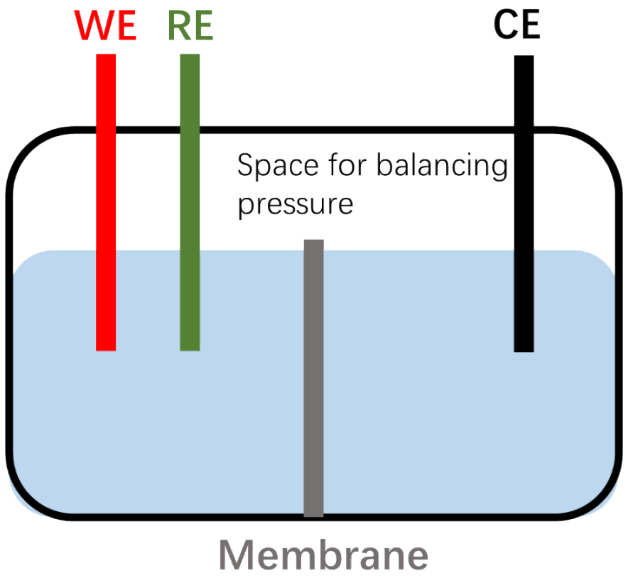

161

162 Fig. S20 A simplified schematic of the high-pressure CO_2RR electrolyzer. The catholyte and anolyte compartments were separated
163 by a membrane, while the shared gas phase was maintained at high CO_2 partial pressures to balance the pressure.

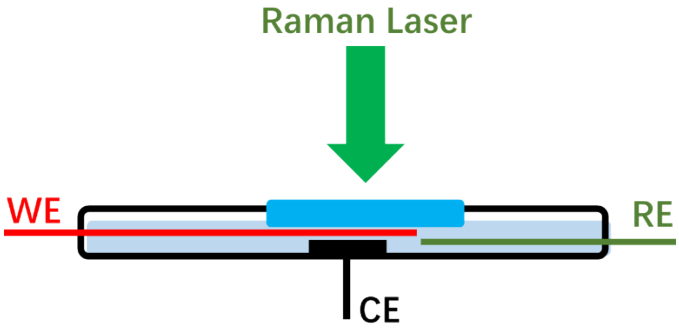

164

165 Fig. S21 A simplified schematic for high-pressure Raman characterization. The high-pressure in situ Raman spectroscopy setup is
166 depicted with a top-view photograph and a side-view schematic. Featuring a three-electrode electrochemical cell housed within
167 a stainless-steel shell and fitted with a sapphire window, the setup facilitates in situ Raman measurements under high-pressure
168 CO_2RR conditions.

Notes and references

1. L. Huang, G. Gao, C. Yang, X.-Y. Li, R. K. Miao, Y. Xue, K. Xie, P. Ou, C. T. Yavuz and Y. Han, *Nature communications*, 2023, **14**, 2958.
2. J. Li, Y. Kuang, X. Zhang, W.-H. Hung, C.-Y. Chiang, G. Zhu, G. Chen, F. Wang, P. Liang and H. Dai, *Nature Catalysis*, 2023, **6**, 1151-1163.
3. G. Kresse and J. Hafner, *Physical review B*, 1993, **47**, 558.
4. G. Kresse and J. Furthmüller, *Sci*, 1996, **6**, 15.
5. G. Kresse and J. Furthmüller, *Physical review B*, 1996, **54**, 11169.
6. P. E. Blöchl, *Physical review B*, 1994, **50**, 17953.
7. G. Kresse and D. Joubert, *Physical review b*, 1999, **59**, 1758.
8. J. P. Perdew, K. Burke and M. Ernzerhof, *Physical review letters*, 1996, **77**, 3865.
9. S. Grimme, S. Ehrlich and L. Goerigk, *Journal of computational chemistry*, 2011, **32**, 1456-1465.
10. D. J. Chadi and M. L. Cohen, *Physical Review B*, 1973, **8**, 5747.
11. V. Wang, N. Xu, J. C. Liu, G. Tang and W.-T. Geng, *arXiv preprint arXiv:1908.08269*, 2019.
12. W. Yi, G. Tang, X. Chen, B. Yang and X. Liu, *Computer Physics Communications*, 2020, **257**, 107535.
13. K. Momma and F. Izumi, *Journal of applied crystallography*, 2011, **44**, 1272-1276.
14. J. K. Nørskov, J. Rossmeisl, A. Logadottir, L. Lindqvist, J. R. Kitchin, T. Bligaard and H. Jonsson, *The Journal of Physical Chemistry B*, 2004, **108**, 17886-17892.
15. J. Zhang, J. Ma, T. S. Choksi, D. Zhou, S. Han, Y.-F. Liao, H. B. Yang, D. Liu, Z. Zeng and W. Liu, *Journal of the American Chemical Society*, 2022, **144**, 2255-2263.